JCTC Journal of Chemical Theory and Computation

Article

pubs.acs.org/JCTC

Protein Effects on the Optical Spectrum of the Fenna–Matthews–Olson Complex from Fully Quantum Chemical Calculations

Carolin König and Johannes Neugebauer*

Theoretische Organische Chemie, Organisch-Chemisches Institut, Westfälische Wilhelms-Universität Münster, Corrensstraße 40, 48149 Münster, Germany

Supporting Information

ABSTRACT: We present a fully quantum-chemical study on the optical spectra of the Fenna–Matthews–Olson (FMO) protein. We have investigated the structural and environmental effects on the site energies and excitonic couplings as well as on the UV/vis absorption spectra. Our largest model of the entire protein–pigment network contains more than 7000 atoms. Structures of all bacteriochlorophyll pigments have been optimized in their binding pockets, comprising more than 1000 atoms in some cases. We find that the site energies are quite sensitive to structural and environmental changes in the model setup, while excitonic couplings are more robust. It is shown that nonoptimized pigment structures lead to site energies closer to the ones for pigments optimized in their binding pocket than to those for conformations fully optimized in vacuum. The determination of reliable site energies is one of the key factors for an understanding of the excited-state properties of the FMO protein.

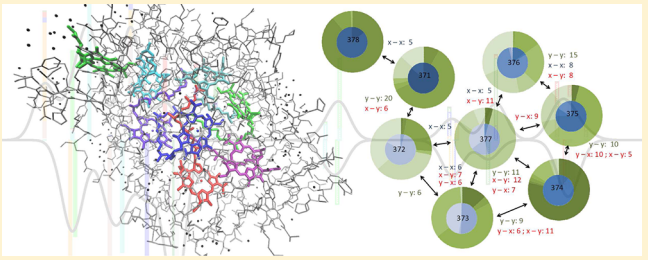

1. INTRODUCTION

The Fenna–Matthews–Olson (FMO) protein[1,2] connects the chlorosome with the reaction center in green sulfur bacteria and is thus essential for the energy transfer in these organisms (see refs 3, 4). It consists of three protein chains, which are arranged in approximate C_3 symmetry. Each of these protein chains forms an envelope comprising seven bacteriochlorophyll (BChl) pigments.[3] An eighth BChl pigment located outside the envelope has been discovered recently.[5,6] In the pdb entry 3EOJ,[5] this site only has an occupancy of about one-third, which might be due to the purification procedure.[5,6] Its plane is oriented roughly perpendicular to those of the other BChl pigments. Optical spectra and energy transfer in pigment–protein complexes such as FMO are determined by the excitation properties of the constituting pigments and their interplay. The theoretical description of excited-state processes usually starts from a single pigment picture. The excitation energies of the pigment are assumed to be modified by the protein environment. The resulting hypothetical local excitation energies are known as site energies. These local excitations interact via excitonic couplings, which can lead to a (partial) delocalization of the excited states. The electronic structure of pigment–protein complexes is thus mainly determined by these two different sets of parameters. However, other factors such as the spectral line shape also can play a role (see refs 7–9 and references therein). In case of the FMO complex, the electronic structure is believed to be mainly dominated by rather localized excitations.[4] Different reported sets of site energies for the FMO protein are gathered and discussed in ref 4. In general, the site energies obtained with different methodologies seem to converge. This holds in particular for the location of the exit pigment; that is, it seems to be accepted that the lowest site energy is that of BChl 373 (see Figure 1). However, the site-energy sets still differ in several details, and a recent theoretical study pointed out that the energy-transfer kinetics calculated with different sets of reported site energies can differ significantly.[10] Despite its rather low extent, delocalization of the excitations is a crucial factor for the description of the energy transfer within the system.[11] In particular, the role of the eighth BChl in the energy transfer is discussed: Its location close to the chlorosome suggests a function as an "energy entry" pigment,[5] which has been supported by quantum-chemical/electrostatic calculations reported by Schmidt am Busch et al.,[12] but questioned in a study taking dynamic considerations into account and employing a structure from a different organism.[13] Thus, there is a strong need for reliable reference data.

Experimentally, the site energies and exciton coupling parameters are typically obtained by fitting time-resolved spectra. Unfortunately, for large systems the number of fit parameters can be too high to be determined unambiguously by fitting to available spectra (see refs 7, 14–17, and references therein). As a physical meaning can be assigned to (most of) the fit parameters, they can be determined using quantum chemical methods. Theoretical studies, however, often suffer from the large number of unknown factors in the model setup that need to be controlled.[8,9,18] Many previous studies aim at a

Received: December 20, 2012
Published: March 1, 2013

dx.doi.org/10.1021/ct301111q | J. Chem. Theory Comput. 2013, 9, 1808–1820

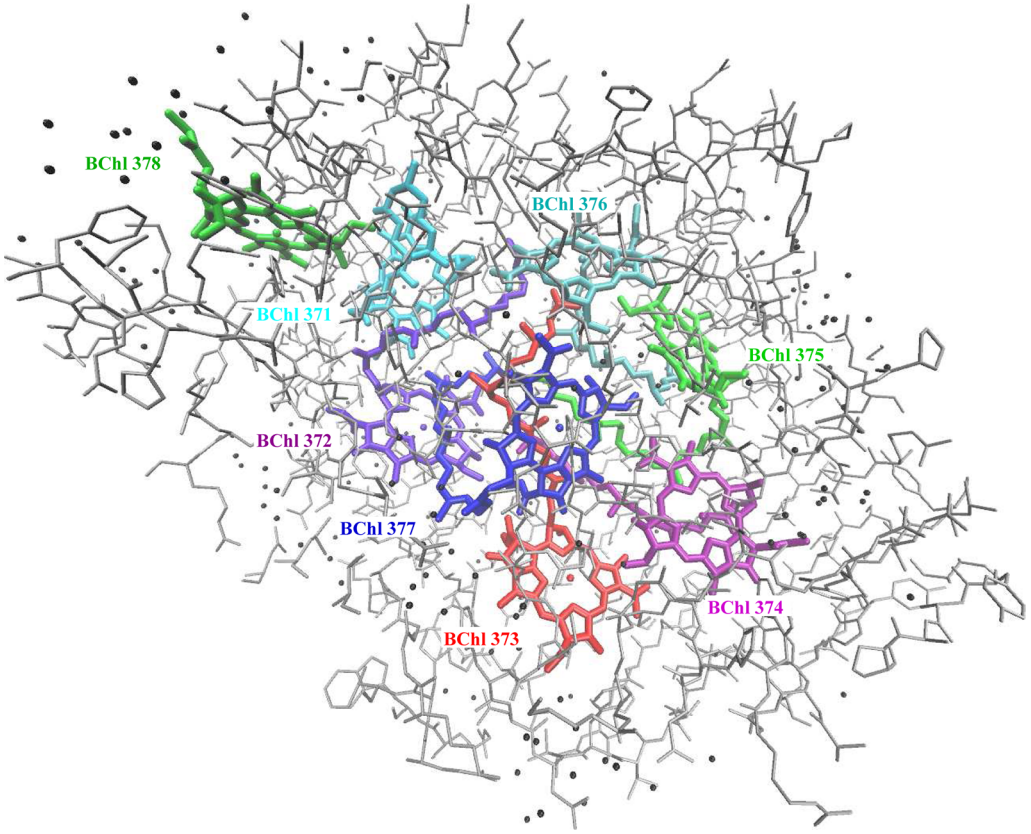

Figure 1. Largest environmental model for the FMO protein in this study with more than 7000 atoms (denoted as "all-10-Å-model"). The hydrogen atoms are not shown, and the water molecules are represented as black dots. The structure was visualized using VMD.[70]

combination of experimental results and theoretical models, that is, obtaining part of the parameters computationally but keep some empirical, system-specific parameters, such as scaling factors for the transition densities and dielectric constants (see refs 8, 19). A reliable approach free of system-specific parameters is desirable, as it would increase the predictive power of the theoretical model. The frozen density embedding (FDE) approach[20] with its extentions to excited states[21,22] offers many advantages in this respect, as it does not contain any empirical parameters apart from the usual parametrization present in the density functionals. Several individual factors have already been addressed in previous studies.[23−25] Here, we are going to take the next important steps by (i) using more realistic structural models for the pigments in their binding pocket, which may comprise more than 1000 atoms in some of our models, and (ii) including most of the protein in the calculation of the site energies.

Many theoretical studies investigating the site energies in photosynthetic complexes account for the environmental effects by means of electrostatics. This is, for instance, done by charge-density coupling[12,26−29] or by including classical point charges in the quantum chemical calculations.[13] Another possibility is to include the environment explicitly in the quantum chemical region.[30] In the latter way, only small parts of the environment can be taken into account, which might cause an unbalanced description. This holds true particularly if unscreened charges are involved, which can lead to a larger range of site energies than experimentally observed.[30] Moreover, when including the environment into the quantum chemical calculations, the electronic structure, and thus the interpretation, is severely complicated. The FDE approach combines the advantages of both methods: It treats the environment quantum chemically but divides the whole system into smaller fragments, which allows to treat much larger systems quantum-mechanically and facilitates easy interpretations.

As shown previously, already small structural differences can lead to quite significant changes in calculated excitation energies of (bacterio-)chlorophyll derivatives.[25,30−34] For instance, different crystal structures for the FMO protein of *Prosthecochloris aestuarii* were shown to yield significantly different results.[31] A reoptimization of the crystal structures is recommended.[35] Still, the steric effect of the binding pocket on the site energies also might be non-negligible and should not be leveled out by a free optimization.[25] Thus, a geometry optimization in the binding pocket should be considered where applicable. The structural question gets even more severe if the available X−ray data contains alternate locations, which means that for some of the atoms more than one position and relative occupancies are provided. Moreover, the positions of hydrogen atoms are usually not resolved in the crystal structure. Hence, an assumption concerning the protonation has to be made, which has a large effect on the electrostatics in the protein[36] and thus can affect the site energies (see refs 8, 25, 26, 29, 30). However, if a non-neutral protonation pattern, such as a physiological protonation pattern, is applied, one should make sure that the system is large enough to allow for sufficient screening of the charges. Even well-screened charges may have a significant impact on many properties of residues in a protein, such as shown in ref 37 for free energies of radical states.

This leads to another aspect of the model setup: the size of the environment taken into account. Here, one needs to find a compromise between the convergence of properties with the

dx.doi.org/10.1021/ct301111q | J. Chem. Theory Comput. 2013, 9, 1808−1820

size of the system and feasibility of the calculations. In ref 28, it was concluded that in case of photosystem I more than 50 amino acids are needed in an electrostatic/quantum chemical approach in order to calculate the electrochromic shift of certain chlorophyll pigments in the protein. However, in most cases, 11 to 20 amino acids were found to be sufficient to converge the site energies. For the FMO protein, the dipole moment of the α helix was suggested to direct the excitonic energy transfer.[38] This interpretation, however, is incompatible with the conclusions drawn by Warshel and co-workers that only the dipole moments in the first one or two turns of a helix significantly contribute to the electrostatic effect of the helix.[39] These authors note that the overestimation of the dipole moment of the helix might be traced back to an underestimation of the effective dielectric constant. Hence, due to several possible choices of protonation pattern, local dielectric constants, and structural factors, a realistic description of electrostatics in proteins is not trivial and might even require averaging over long trajectories, as concluded in refs 40 and 41. A review on electrostatics in proteins can be found in ref 36.

The second key parameter, the excitonic coupling, can be calculated with a number of different approximations related to the first formulation of excitonic energy transfer by Theodor Förster in 1948.[42] The interested reader is referred to refs 8, 9 and 43 for an overview. Methods mentioned later in this article are the dipole−dipole approximation[42] and the transition charges from the electrostatic potentials (TrEsp) method.[44] In the first, excitonic couplings are expressed as an electrostatic interaction of the corresponding transition dipole moments, while in the latter method the transition densities are represented in terms of (usually atom-centered) partial transition charges.[44] In this work, we will employ the extension of the FDE scheme to coupled excited states (subsystem TDDFT)[22] to calculate exciton coupling parameters. Since the eigenvalues of the (subsystem-) TDDFT eigenvalue problem are the squared excitation energies, the coupling matrix elements in subsystem TDDFT cannot directly be interpreted as exciton coupling parameters. This is why we reconstruct the configuration interaction singles (CIS)-like exciton coupling parameters from a 2×2 matrix eigenvalue problem containing local (FDEu) excitation energies and delocalized (FDEc) excitation energies, as described in ref 23. The sign of these coupling matrix elements is chosen according to the sign of the corresponding subsystem-TDDFT coupling matrix element. However, for larger aggregates, a number of different consistent sets of signed exciton couplings elements can be generated, due to the free choice of sign for each wave function. Therefore, we focus on the unsigned exciton couplings containing the main information on the strength of the coupling in the main text. Signed exciton coupling parameters are given in the Supporting Information.

The FDE approach applied here[22] thus connects the terms "site energies" and "excitonic coupling" to calculations in the same framework, that is, uncoupled FDE (termed "FDEu") and coupled FDE (termed "FDEc"). It is a consistent approach for the calculation of optical spectra of protein−pigment complexes such as light-harvesting complexes; see also refs 23 and 25. In our analysis, we focus on the structural and technical effects on the delocalization of the excitations within the pigment network in the FMO protein. Besides conformational aspects, we mainly investigate the effect of an increasing environment. The largest model employed here contains all eight bacteriochlorophyll pigments optimized in their individual binding pocket and all residues in a distance of 10 Å from one of these pigments, including residues from neighboring protein chains. The number of atoms in this model exceeds 7000 atoms, which are all treated by means of density functional theory (DFT). This is currently, to the best of out knowledge, the largest application of FDE.

This article is organized as follows. After discussing details of the computational method and model setup in Section 2, we will discuss the determination of the site energies. In particular, we will investigate the effect of the choice of alternate location (Section 3.1), optimization strategy, and treatment of the environment (Section 3.2). In the discussion on the delocalized electronic structure in Section 3.3 we will, after showing two example cases, compare the obtained excitonic coupling constants and spectra. Besides discussing technical aspects, we will comment on the capability of the models and approach applied here to describe and predict the physics in the real system. For the latter point, we will mainly focus on our largest models, comprising all pigments optimized in their individual binding pocket and the major part of the protein. Finally, we will conclude and give an outlook in Section 4.

2. METHODS AND OPTIMIZATION STRATEGIES

2.1. Computational Details. If not specified otherwise, we employed the TURBOMOLE[45] program package for geometry optimizations. These calculations were carried out with the Becke−Perdew functional (BP86),[46,47] a triple-ζ basis with valence polarization (TZVP), and applying the resolution-of-the-identity (RI) approximation as the default. For additional geometry optimizations in a DFT/density functional tight binding (DFTB)[48−50] hybrid scheme, we employed the QUILD[51] module of a locally modified version of the Amsterdam Density Functional (ADF) program package and the BP86 functional in combination with the triple-ζ basis set with one set of polarization functions for all atoms (TZP). In these calculations, frozen 1s core orbitals ("small cores") were employed for the C, N, O, and Mg atoms in the DFT part.

The excited-state calculations were by default performed with a modified version of ADF[52] applying the "statistical averaging of (model) orbital potentials" (SAOP) potential[53−55] and the TZP basis set. We have compared different electronic-structure methods for chlorophyll residues in the light-harvesting complex II (LHC-II) of green plants previously.[25] For these examples, we have found that the effect of structural differences on the excitation energies are predicted to be very similar with TDDFT (SAOP/TZP), with hybrid and double hybrid functionals as well as with wave function-based methods such as CIS and CIS(D).[25] These findings provide confidence that SAOP/TZP is a reasonable choice also for bacteriochlorophylls (BChls) as present in the FMO protein. In case of FDE calculations, we employed the so-called GGA97 generalized-gradient approximation (GGA) for the nonadditive kinetic contribution to the embedding potential.[56] For these calculations, we employed the ADF implementation of FDEu[57,58] and the FDEc formalism.[22] If not specified otherwise, we performed three so-called freeze-and-thaw cycles[59] in the FDEu calculations, as was found sufficient to converge the excitation energies in a similar case.[25] However, due to the computational expenses, we only performed one freeze-and-thaw cycle for the largest model ("all-10-Å-model", see below) and recomputed the pigments' properties afterward. The first freeze-and-thaw cycle has been shown to cover the major polarization effect.[25,57] For relative energies such as the

site energies calculated here, an even better convergence can be expected.

2.2. Bacteriochlorophyll Models and Optimization Strategies. The structural models used here are all based on the currently best resolved FMO crystal structure from *Prosthecochloris aestuarii* (pdb code: 3EOJ, resolution: 1.30 Å).[5] The missing hydrogen atoms were added according to the known connectivities of the residues, in such a way that all residues are neutral. This protonation pattern has been chosen since most of our models do not include the entire protein nor a surrounding medium. Thus, charges might not be screened properly, so that a neutral protonation pattern resembles the real charge distribution better than possibly unscreened charges.

The pdb entry 3EOJ contains alternate locations (labeled as A, B, C, D, E, and F) for a number of atoms, which also includes atoms in BChl and amino acid residues in their environment. For this work, we have chosen the combination of alternate locations A, D, and F (referred to as A-D-F) as this represents the structure with the highest population of sites, and the alternate locations B, D, and F (referred to as B-D-F) because the eighth bacteriochlorophyll (BChl 378) only occurs in the alternate location B.

In some cases, we have replaced the phytyl chain by a hydrogen atom (truncated model), which has been reported earlier to lead to only small changes in the excitation energies.[25,60] Subsequently, we optimized the pigments' geometries employing the following optimization strategies:

- optH: truncated model; only hydrogen atoms optimized (TURBOMOLE/BP86/TZVP). For these truncated models, only the structures of residues 376, 377, and 378 differ from A-D locations to B-D locations in this scheme.
- optA: truncated model; all atoms optimized (TURBOMOLE/BP86/TZVP). Here, the same number of different A-D and B-D structures occur as in the optH scheme.
- optP: geometry optimization of the complete BChl molecule in a pocket applying the following procedure
  1. cut pockets of 4 Å radius (before adding the H atoms; consider also neighboring protein chains).
  2. identify molecular subunits.
  3. combine water molecules with close-by residues containing H-bond acceptors to new subunits.
  4. protonate molecules to achieve neutral protonation pattern.
  5. optimize hydrogen positions for each fragment separately (TURBOMOLE/BP86/TZVP).
  6. geometry optimization with QUILD: DFT(ADF/BP86/TZP[small core]) for the chlorophyll and DFTB(TZP[small core]) for the entire frozen protein pocket.

  The A-D-F and B-D-F optP structures are not identical in any case, as every binding pocket of the BChl residues contains alternate locations that differ for A and B.

  In case of BChl 376 with the A-D-F and B-D-F pocket, respectively, no convergence with QUILD using strict optimization criteria (gradient to 0.001 hartree/bohr) could be achieved. For both cases we performed TDDFT (SAOP/TZP) calculations for different structures with small energy gradient in the final stage of optimization. This was done in order to analyze whether the excitation properties are converged, which was the case for the B-D-F location but not for that with the A-D-F alternative. In most other cases, the differences in excitation energies between the A-D-F and the B-D-F pocket are small. Among the A-D-F structures with a small energy gradient, we therefore chose that one giving rise to excitation energies similar to that obtained for the corresponding B-D-F structure.
- optP(trunc): similar to optP but for the truncated model. The hydrogen atom which replaces the phytyl chain was separately optimized (ADF/BP86/TZP[small core]). For BChl 378, this is the same as optP.

The largest model in this study was generated by taking all residues with at least one atom closer than 10 Å to one atom in the truncated chlorophyll (not considering the hydrogen atoms). This model was only generated for the B-D-F alternate location. The hydrogen atoms were optimized (BP86/TZVP) for each covalently bound subunit and all water molecules together with the sodium cation, respectively. Subsequently, these structural models were combined with the complete optP BChl structures to a model containing more that 7000 atoms. This model is shown in Figure 1 and will be termed "all-10-Å-model" in the following. The structures of the 4 Å pockets for each subsystem can be found in Figure SI-1 in the Supporting Information.

3. RESULTS AND DISCUSSION

We investigated the impact of several factors on the electronic structure of the BChl network in the FMO protein. Among the factors considered here are the pigment structures as well as effects of the environment. The applied structural models are discussed in detail in Section 2.2. To account for environmental effects, we either included all other BChl pigments of the same type of structural model (FDEu network), the complete steric pocket for this pigment (FDEu pocket), or all atoms of the all-10-Å-model into the FDEu calculations. The crystal structure contains a number of different alternate locations, which also affect the BChl pigments and their environment. Hence, we will first describe the effect of the choice of alternate location for BChl 376 and 377 in Section 3.1. Subsequently, we will discuss the site energies calculated for all mentioned structural and environmental models and compare them to results by other authors based on empirical models of the protein environments in Section 3.2. In Section 3.3, we will first present the information on the electronic structure of the pigment network that can be extracted from the FDEc calculations. We will then continue with a comparison of the excitonic couplings for the different models in Section 3.3.1. The resulting delocalized excitations and optical spectra are subsequently discussed in Section 3.3.2.

3.1. Alternate Locations. For the BChl residues 376 and 377 the pdb entry 3EOJ contains the alternate locations labeled A, B, C, and D in the bacteriochlorophyll ring. In both cases, there are four possible structures for the truncated model, which are A-C, A-D, B-C, and B-D. We have calculated the excitation energies and oscillator strengths for the truncated optH structures of all possible alternate locations in these truncated models for BChl 376 and 377. These calculations result in differences for the Q_y excitation energies of up to 0.024 eV [BChl 377 (A-D)−(B-C)] and for Q_x of up to 0.030 eV [BChl 377 (A-C)−(B-D)]. The larger change in Q_x excitation energies compared to that in Q_y excitation energies is in line with the stronger sensitivity of the Q_x excitation to axial

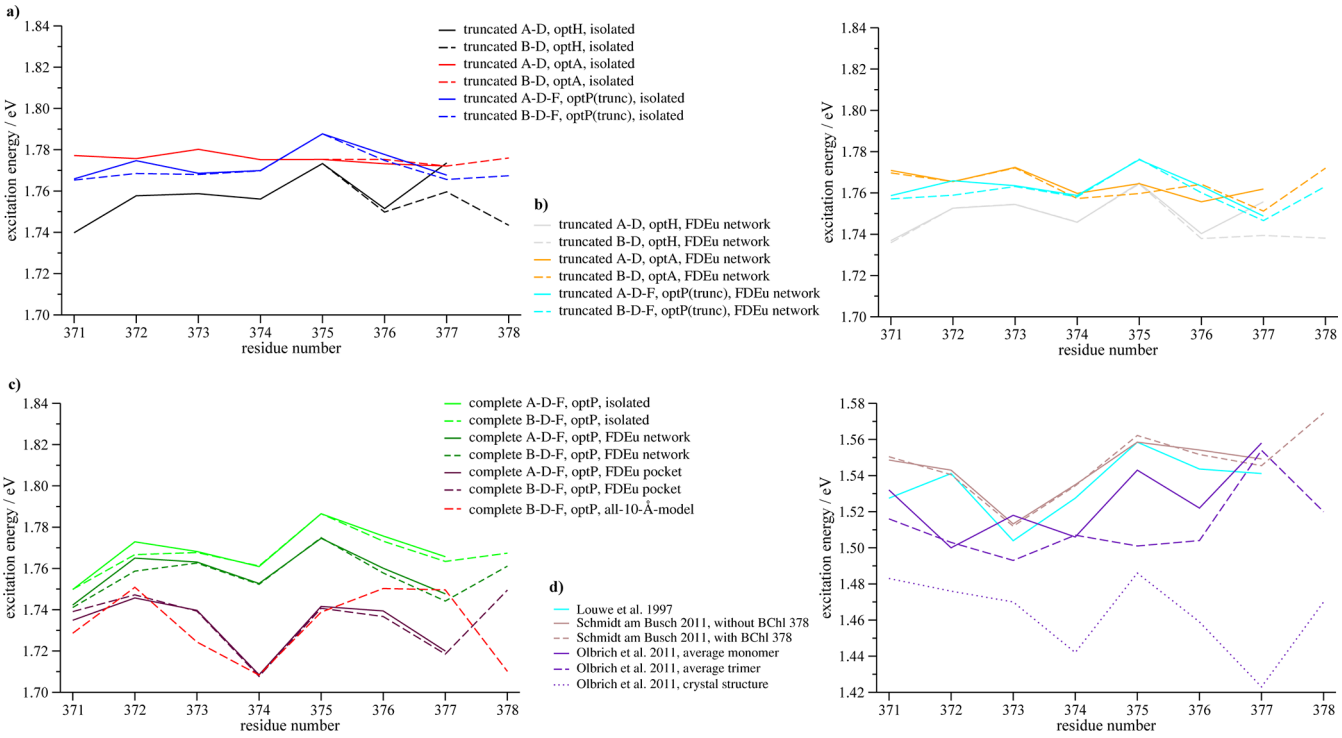

Figure 2. Calculated site energies with different structures [(a) and (b) truncated structures, (c) complete structures] and considerations of the environment, that are none (isolated), relaxed with respect to the BChl network (FDEu network), relaxed with respect to the steric pocket (FDEu pocket), or relaxed within the entire all-10-Å-model. (d) Data from earlier studies by Louwe et al.,[63] Schmidt am Busch et al.,[12] and Olbrich et al.[13] for comparison.

ligation, that is, nonplanar distortion of the aromatic ring.[9,23,61,62] The oscillator strengths differ by up to 0.02 [Q_y; BChl 377 (A-D)−(D-B)]. For details see Table SI-I in the Supporting Information.

3.2. Site Energies. In this section, we discuss the impact of different structural and environmental aspects on the site energies of the pigments. For the sake of brevity, we will restrict ourselves to the discussion of the Q_y excitation energies. The corresponding oscillator strengths and the data for the Q_x excitations can be found in Table SI-II in the Supporting Information.

The calculated Q_y excitation energies for all pigments obtained with different combinations of structures and treatment of the environment are plotted in Figure 2. Figure 2a shows the Q_y excitation energies calculated for the isolated truncated models and Figure 2b contains the results of the FDEu-network calculations for the same models. In Figure 2c, the Q_y excitation energies for the complete models are plotted, and Figure 2d contains earlier reported data.[12,13,63] The continuous lines represent the set of calculations for the A-D-F locations, and the dashed lines those for the B-D-F alternative. For BChl 378 only in the latter sets site energies are included as this residue is only present in the B alternate location. In the case of isolated optH and optA structures, the only differing residues present in both sets are BChl 376 and BChl 377. The calculated differences are generally rather small (about 0.002 eV) for BChl 376 but larger (0.014 eV) for BChl 377. Also, for most optP structures, the Q_y excitation energies for A-D-F structures differ only little from that of the B-D-F structures. The Q_y excitation energies calculated with the optP structures for BChl 372 for the different pockets are exceptional: They differ by 0.01 eV.

Comparison of the different optimization strategies shows that the spread in site energies is reduced if the structure of the pigments is optimized: It decreases from 0.034 eV for the optH structures to <0.010 eV for the optA structures. The Q_y excitation energies of the latter are shifted to higher energies. The range for the optP(trunc) structures lies in between these values. It amounts to 0.022 eV, and the trend for BChl 372 to BChl 376 mainly resembles that of the optH structures. Nevertheless, the impact of the optP optimization on the excitation energies differs for different pigments: The relative Q_y excitation energy for BChl 371 is increased and that of BChl 377 significantly lowered for the optP(trunc) structures compared to the optH structures. Also, the Q_y excitation energy of BChl 378 calculated for the optP(trunc) structure is shifted to higher excitation energies with respect to that obtained with the optH structure. In case of the complete optP structures, the relative trends remain similar to that for the optP(trunc) structures, but the spread is increased to 0.037 eV. It is thus higher than that for the truncated optH structures. The neglect of the phytyl chain in excitation-energy calculations on chlorophyll pigments has been justified by only small changes in the calculated excitation energies and oscillator strengths.[25,60] However, in the case of site energies in photosynthetic complexes, we are interested in rather small energy deviations, so that the effect of the phytyl chain might not be generally negligible. Moreover, our findings might indicate that the optH scheme can be advantageous over the optA scheme and thus be the method of choice if a geometry optimization considering sufficient part of environment is not affordable. However, this should be done with caution, as the effect can be different for different pigments in one system. For a similar system, that is, a chlorophyll dimer from the LHC-II, it is reported that a reoptimization of the crystal structure is

dx.doi.org/10.1021/ct301111q | J. Chem. Theory Comput. 2013, 9, 1808−1820

essential to obtain reliable excitation energies.[35] However, also, there it was stressed that the reoptimization needs to be done with constraints keeping the relative orientation of the pigments.

When going from the isolated to the FDEu-network results, the spread in the site energies of the optH and optP(trunc) structures is in most cases decreased, while that of the optH structures is increased. Accounting for the binding pocket as environment (FDEu pocket) leads to an increased spread in excitation energies of 0.040 eV; see Figure 2c. If we exclude BChl 374 and BChl 377 from that set, all Q_y excitations lie in a range of 0.010 eV. This is the only set of site energies calculated here in which BChl 378 has the highest site energy. The situation is quite different for the all-10-Å-model. Compared to the FDEu-pocket calculations, the site energy of BChl 373 is lowered by 0.015 eV but is still higher than that of BChl 374. A similar shift of 0.011 eV is obtained when employing a pocket of 10 Å solely around this pigment (three freeze-and-thaw cycles, data not shown); that is, contrary to earlier findings (see refs 4, 12, and 63), our calculations suggests the BChl 374 to be the lowest-energy site (for a more detailed comparison, see below). The most striking differences between the FDEu-pocket site energies and those for the all-10-Å-model are obtained for the residues BChl 376 to 378. In the all-10-Å-model calculations, the site energies of BChl 376 and 377 are increased by 0.013 and 0.031 eV, respectively, compared to the FDEu-pocket results. That of BChl 378 is decreased by 0.040 eV. In particular, the site energy of BChl 378 seems to be inconsistent with the other sets of site energies. The difference in site energies for the different models for this particular pigment can be rationalized by its peripheral location pointing to the baseplate of the chromosome in the organism.[5] In the crystal structure, this peripheral location is accompanied with an accumulation of water molecules on that side of this pigment where in the organism the baseplate is attached. Thus, the deviation might be caused by the inclusion of more of these water molecules in the all-10-Å-model than in the FDEu-pocket calculations and is, thus, most probably an artifact of this model. Removing all water molecules and the sodium cation from the FDEu calculation of BChl 378 (keeping all other densities as in the all-10-Å-model) resulted in an increase of 0.010 eV in the excitation energy. This supports the interpretation that the low site energy of BChl 378 in the all-10-Å-model is partially due to the accumulation of water residues on one side. However, it does not explain the whole shift compared to the FDEu-pocket calculations. Still, for the more central pigments such as BChl 377, we think that the all-10-Å-model results in more physically reasonable results than the smaller models. This is supported by the observation that relative site energies of BChl 376 and BChl 377 obtained in the all-10-Å-model fit better to the earlier reported sets (see below) than those from the FDEu-pocket model. An overview over the spectral range of excitation energies and oscillator strengths calculated for the Q excitations of all sets discussed here can be found in Table SI-III in the Supporting Information.

In conclusion, the spectral range of site energies for the truncated models decrease in the order optH > optP(trunc) > optA, which is in line with an earlier study on the chlorophyll pigments in the LHC-II.[25] This also holds for the effect of accounting for the FDEu network. It leads to a decreased spread of the site energies in case of the optH structures and an increased spread for optA structures.

Figure 2d shows site energies for FMO calculated in two earlier theoretical studies by Schmidt am Busch et al.[12] and by Olbrich et al.[13] In addition, a set of fitted site energies by Louwe et al.[63] is included. It is worthwhile to mention that the studies by Schmidt am Busch et al. and Louwe et al. investigate the FMO protein from the same species as in this study (*Prosthecochloris aestuarii*) and Schmidt am Busch et al. even employed the same pdb entry. The study by Olbrich et al. is based on the pdb entry 3ENI, that is, on a structure from *Chlorobaculum tedium*. The structures differ in important details. For instance, in 3ENI, the magnesium ion of BChl 378 is only coordinated to an amino acid on one side, while it has two axial ligands in 3EOJ. Structural differences in the pigments' environment in different species have been put forward as an explanation for the differences in the optical spectra and energy transfer in these species.[5,64] We chose the data from Louwe et al.[63] as an experimental reference. This set of site energies contains, according to ref 4, the "most widely accepted values". That study has been carried out before the eighth BChl pigment was found. Consequently, site energies are only given for BChl 371 until BChl 377. Comparison of the previous data shows that the experimental values obtained by Louwe et al. agree very well with those by Schmidt am Busch et al.[12] The only exception is that of BChl 371, which is somewhat lower in energy in the set by Louwe et al. compared to that by Schmidt am Busch et al.[12] The site energies calculated for a monomer of the FMO protein of *Chlorobaculum tedium*,[13] however, hardly show similarity to the other studies, while those calculated for the trimer result in the same "exit pigment" (BChl 373), as found in a number of other studies (see ref 4 and references therein). A more extensive discussion on reported site energies for the FMO protein and the differences in determining them can be found in refs 4 and 13. Compared to our data, the site energies from the previous studies are lower by about 0.2 eV. This deviation lies within the typical error bar of valence excitations determined with TDDFT (see ref 65 and references therein) and is thus possibly explainable by the use of another computational method (TDDFT/B3LYP in refs 12 and 38 and ZINDO/S-CIS in ref 13).

We observe similarities between the set of site energies for the crystal structure by Olbrich et al.[13] to our optP data, which might again underline the impact of the pigment structures on the site energies. Nevertheless, we will, due to the described complications and similarities, restrict our further comparison to the data to Schmidt am Busch et al.[12] The site energies reported in that study span a range of 0.063 eV (considering BChl 378) and 0.045 eV (without BChl 378), respectively, which is larger than the one obtained in this work. A major difference is also observed in the site of the lowest site energy, that is, the exit-pigment. In our most elaborate calculations, that is, the all-10-Å-model, the lowest site energy is located at BChl 374, while Schmidt am Busch et al. located it at BChl 373. The latter is in agreement with earlier experimental data (see ref 4 and references therein). Also, the location of the highest site energy at BChl 378, reported in ref 12 is not reproduced with the all-10-Å-model. However, BChl 378 is the highest-energy site in our study when considering separate binding pockets of 4 Å radius. As discussed, the low site-energy of BChl 378 in the all-10-Å-model might be an artifact of that model.

3.3. Coupled Network. For all combinations of structural and environmental models mentioned in the previous section we have performed FDEc calculations to investigate the

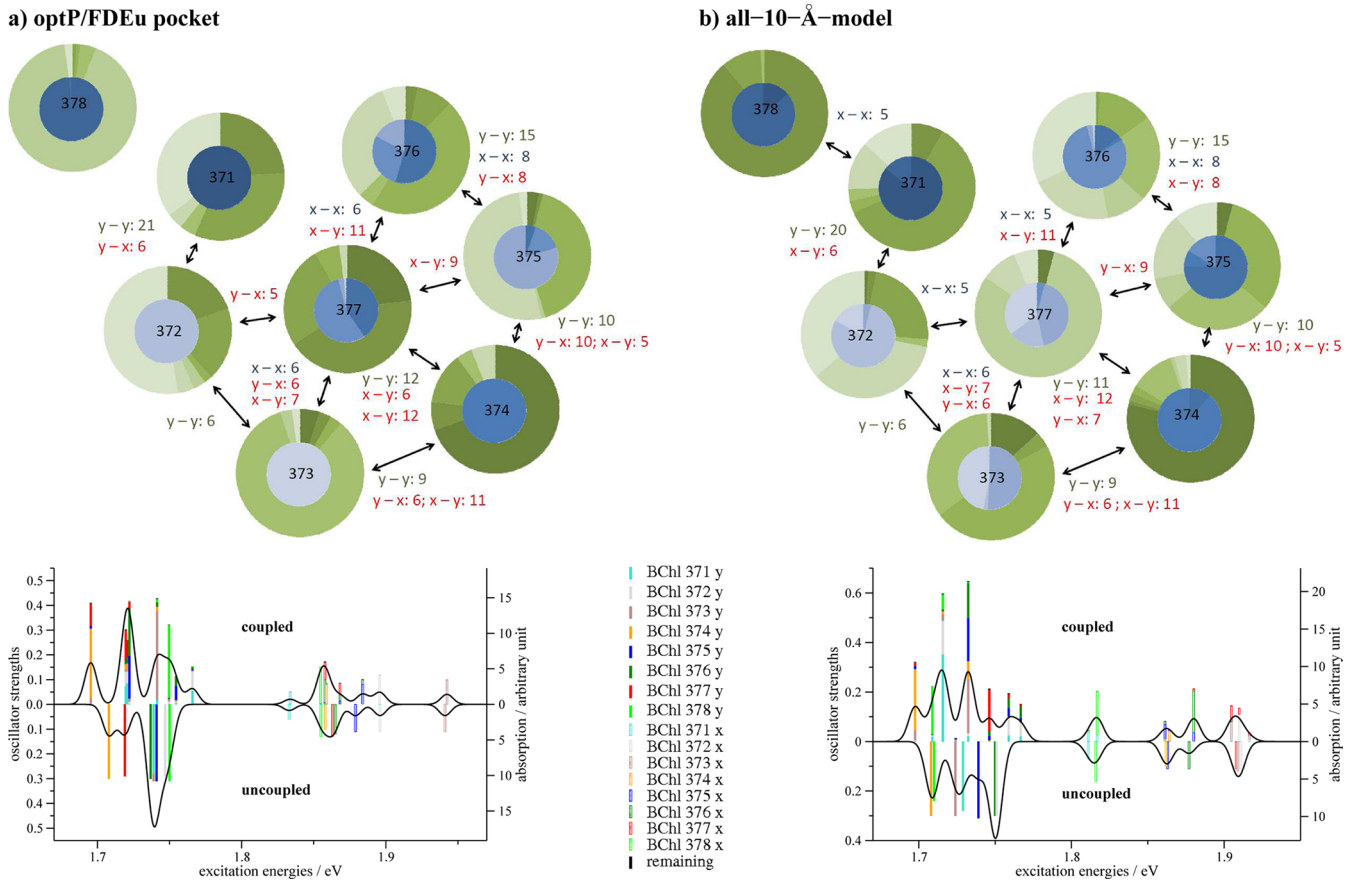

Figure 3. Visualization of the outcome of an FDEc calculation (SAOP/TZP) for the complete optP B-D-F structure and local excitations from (a) FDEu-pocket calculations and (b) the all-10-Å-model. Top: spatial structure of the delocalized excitation and coupling constants in meV. Bottom: effect of coupling on the optical spectra. The stick spectra were broadened with a Gaussian line shape and a half width of 0.01 eV. For a more detailed description, see the main text.

characteristics of the excitonically coupled system. It should be noted that in the FDEc implementation fully converged electron densities for the systems to be coupled are assumed. That means that the FDEc calculations employing local excitations which are not relaxed within the same system as chosen for the coupling (i.e., those from isolated, FDEu pocket, and the all-10-Å-model calculations) are, from a methodological point of view, not fully consistent.

The outcome of an FDEc calculation is visualized in different ways in Figures 3 and 4. The examples shown correspond to the most elaborate calculation, that is, those for the complete B-D-F optP structures with either the pocket of 4 Å radius or the all-10-Å-model. In the upper part of Figure 3, each set of a green and a blue pie chart represents one pigment in the network. The pie charts are arranged such that they reflect the relative locations in the network as shown in Figure 1. The numbers attached to the arrows are the excitonic coupling constants (in meV) between the Q excitations of the pigments; only those larger than 5 meV are shown. The pie charts show the contributions of the localized Q_y (green) and Q_x (blue) excitations to a coupled excitation, where the darkest color represents the lowest coupled excitation of this type. In most cases, the Q_y and Q_x excitations are quite well separated, which allows this type of visualization. It gives an overview on how the excitations of the coupled system are spatially delocalized over the network. In both models, the lowest excitation has the largest contribution from BChl 374, which coincides with the lowest site energy, but significant contributions are also found at BChl 377, 373, and 375 (for optP/FDEu pocket) and only at BChl 373 in case of the all-10-Å-model. For the latter pigments, we obtain significant Q_y excitonic couplings to BChl 374. A comparison of these two models shows that despite the very similar exciton coupling parameters, the distribution of the local excitations on the delocalized ones are quite different. The most striking difference is probably that the excitation localized on BChl 378 is in the higher energy range in case of optP/FDEu pocket and at lower energy for the all-10-Å-model. The most striking similarity is the localization of the lowest excitation at BChl 374. These observations are in accordance with the similarities and differences in the corresponding sets of site energies.

Following the idea of energy transfer along an energy funnel, we observe in both cases that the contributions of higher-energy Q_y excitations are decreased and that of lower-energy Q_y excitations are increased when going from BChl 372 to BChl 374. The energy transfer within the FMO complex is often described in terms of a hopping mechanism, that is, dominated by rather localized excitations.[4] In contrast, we find rather delocalized excitations. This can be due to the neglect of the nuclear motion and the resulting vibrationally triggered localization of the excitations. Still, the contributions of the local excitations in our model could give hints on possible "routes" of the energy transfer. The bar charts in Figure 4 show the contribution to the delocalized Q_y excitations arising from

dx.doi.org/10.1021/ct301111q | J. Chem. Theory Comput. 2013, 9, 1808−1820

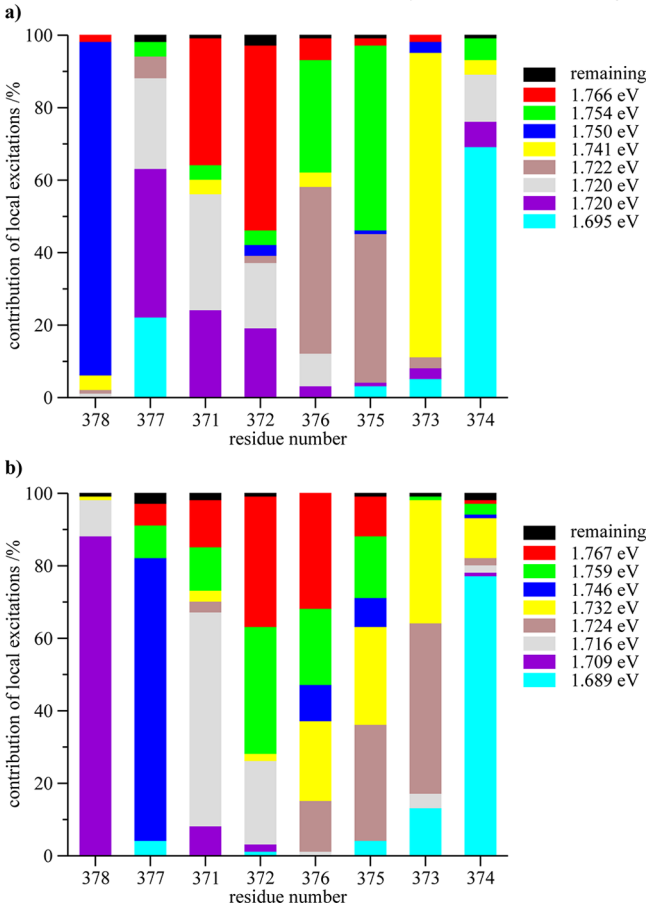

Figure 4. Distribution of the local excitations from (a) FDEu-pocket calculations and (b) the all-10-Å-model on the delocalized excitations (SAOP/TZP). The different colors label the delocalized excitations in the complex, denoted by their excitation energies.

different sites. Here, we have ordered the residues on the abscissa according to possible energy transfer routes (see below) rather than their residue numbers. For both, the optP/FDEu pocket and the all-10-Å-model, the main contribution of the highest-energy exciton state is on BChl 372. The results for the all-10-Å-model indicate a possible transfer of the excitation energy along BChl 376, 375, and 373, that is, the peripheral pigments, to BChl 374. In this case, the role of the central pigment (BChl 377) is not clear. A possible explanation is that it is essential for mediation of the exciton coupling between the other involved pigments. The optP/FDEu pocket calculation suggests a different possible transfer pathway from the BChl 372 to BChl 374, that is, along the central pigments BChl 371 and BChl 377. According to the results for the all-10-Å-model an additional transfer route could be along BChl 371 to BChl 378, that is, into the opposite direction. This is likely be caused by the probably accidentally low excitation energy of BChl 378 in that model. In contrast to that, the BChl 378 appears rather isolated in the optP/FDEu pocket results.

In conclusion, both models do not agree with a picture of localized excitations, most probably because of the missing effect of nuclear motion. Still, the idea of the energy funnel suggests energy transfer routes from BChl 372 to BChl 374 in both models, but the predicted routes differ. Since the all-10-Å-model is the most realistic model in this study, we expect the most reliable results from it. As discussed and rationalized above, the site energy of BChl 378 seems to be predicted too low in the all-10-Å-model. The resulting excitation transfer into the direction of that pigment is thus most probably an artifact of that model. The disagreement of the exit pigment in this study (BChl 374) to the results of earlier studies (BChl 373)[4,12] coincides with differences in the lowest-energy site.

The bottom part of Figure 3 visualizes the effect of the excitonic coupling on the optical spectra of the pigment network. The upside-down spectrum shows the superimposed spectra of the uncoupled FDEu-pocket excitations for all pigments in the network. In the underlying stick spectrum, the color of the sticks refers to the pigment the excitation is localized on whereas the filling of the stick indicates whether it is a Q_y or a Q_x excitation. In the uncoupled spectra, the Q_y oscillator strengths are similar for all pigments, whereas those of the Q_x excitations show larger variations. In the "coupled" spectra, the outcome of the FDEc calculations are shown. The contributions of the localized excitations to the delocalized ones are indicated in the same colors as used for the strictly localized excitations in the upside-down spectra. The coupled spectra show larger variations of excitation energies and oscillator strengths. This effect is clearly more pronounced for the Q_y than for the Q_x bands. In this type of visualization, the separation between the Q_y and Q_x regions is easily recognized.

Before we compare these calculated spectra, we will discuss the main features of the interplay between the site energies and excitonic coupling parameters in the coupled spectra for each model separately. We should keep in mind that the interaction is mainly governed by energetical proximity and the excitonic couplings. Hence, we expect strong interaction and therefore mixing between local excitations in case of very similar excitation energies and large excitonic couplings:

In the optP/FDEu pocket calculations, the local Q_y excitations of BChl 371 and BChl 372 differ by 0.012 eV, and their coupling constant amounts to 21 meV. In the delocalized spectrum, these local excitations are mainly distributed over three delocalized excitations with maximum energy difference of 0.046 eV. The lower two of these three excitations are almost degenerate and have an additional contribution from the Q_y excitation of BChl 377. The excitation energies of these coupled excitations nearly coincide with the uncoupled Q_y excitation energy of BChl 377, which can lead to noticeable mixing in spite of the small excitonic coupling. The localized Q_y excitations of BChl 371 and BChl 373 are almost degenerate but hardly mix in the coupled spectra. This is probably due to the longer distance and the resulting small excitonic coupling. Stronger interactions are observed for the Q_y excitations of BChl 375 and BChl 376, which are energetically separated by only 0.004 eV and coupled by 15 meV. Also, for the Q_y excitations of BChl 374 and BChl 377, a significant interaction is observed. In this case, the local excitations differ in energy by 0.012 eV and the excitonic coupling amounts to 12 meV.

In the all-10-Å-model, the strongly coupled BChls 371 and 372 (coupling constant: 20 meV) have Q_y site energies differing by 0.022 eV. In the coupled spectra, these two local excitations spread over three delocalized ones with energetic differences of up to 0.051 eV. The lowest of these bands is one of the two most intense mixed bands. The Q_y site energies of BChl 374 and 378 are almost degenerate but hardly mix due to a large distance accompanied with negligible coupling constant. Yet, the excitation dominated by BChl 374 is red-shifted by 0.010 eV in the coupled spectrum. This is most probably due

dx.doi.org/10.1021/ct301111q | J. Chem. Theory Comput. 2013, 9, 1808−1820

to the coupling to the Q_y excitations of BChl 373 (9 meV) and BChl 375 (10 meV). The latter local excitations and the Q_y excitation of BChl 376 (which couples to that of BChl 375 by 15 meV) give the largest contributions to the most intense exciton band. The Q_y excitation of BChl 377 (in the uncoupled stick spectrum hidden under the Q_y signal of BChl 376) hardly mixes, despite its rather pronounced couplings to other pigments and its near-degenerate Q_y site energy with BChl 376. This might be another indication for the mediating role of this pigment in this model.

As can already can be seen from Figure 3, the eighth pigment is only weakly coupled to the rest of the system according to both calculations. Thus, this excitation mainly remains unaffected by the coupling, which is in line with the conclusions drawn in refs 12, 13 and 66. With regard to the Q_x excitations, significant couplings are only observed between the Q_x excitations of BChl 375, BChl 376 and BChl 377 in the optP/FDEu pocket calculations. In the case of the all-10-Å-model additional, significant Q_x interactions are observed for BChl 372 and BChl 373.

A comparison of the coupled spectra of the two methods reveals again the sensitivity on the site energies. The Q_y site energies are more homogeneously distributed over the energy range in case of the all-10-Å-model than in the optP/FDEu pocket calculations. For the coupled spectrum, we observe larger deviations of oscillator strengths in case of the all-10-Å-model than in the optP/FDEu pocket calculations. Moreover, the Q_y-Q_x gap is bridged by red-shifted Q_x excitations in the spectrum for the all-10-Å-model.

Figure 5 shows a comparison of the Q_y region of the optical spectrum of the FMO protein calculated here with the optP/FDEu pocket and the all-10-Å-model to an experimental spectrum at 4 K.[14] Since we aim to compare relative excitation energies and line shapes rather than absolute excitation energies, the spectra are shifted in such a way that the major peaks lie in the origin. This corresponds to an offset of 0.20 eV between the experimental and the calculated spectra, which is within the typical error bar of TDDFT for absolute excitation energies. Both calculated spectra are in fair agreement with the experimental one. Especially, the spectra calculated with the optP/FDEu pocket model resembles the experimental one rather well. The better agreement at about 0.03 eV from the maximum in the optP/FDEu pocket model can be related to the apparently better site energy for BChl 378. In any case, this comparison should be done with caution, as quite different electronic structures may lead to similar optical spectra (see also the discussion on the more technical effects on optical spectra in Section 3.3.2), and vibronic effects are completely neglected in our treatment.

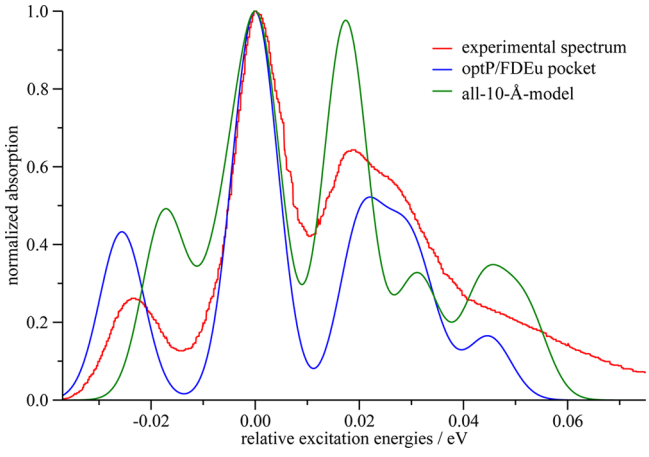

Figure 5. Comparison of the calculated spectra from optP/FDEu pocket calculations and the all-10-Å-model to an experimental spectrum. The experimental spectrum of the FMO protein of *Prosthecochloris aestuarii* at 4 K was reconstructed from data extracted from Figure 1.1 in ref 14. The calculated spectra were broadened with a Gaussian line shape with a half width of 0.01 eV. For better comparison, all spectra were normalized, and their major peak was shifted to the origin; that is, the experimental spectrum has been shifted by −1.518 eV, the optP/FDEu pocket spectrum by −1.721 eV, and that of the all-10-Å-model by −1.715 eV.

In the following, we will first discuss the Q_y excitonic coupling constants for the set of local excitations for the complete optP structures with FDEu pocket and all-10-Å-model, respectively. These models correspond to the most elaborate model setups. Then, we will compare these results to values obtained in earlier studies. Subsequently, we will give a brief overview over the results obtained with the all 19 combinations of optimization strategy and treatment of the environment discussed in Section 3.2 in context of the corresponding site energies. For the discussion, we will restrict ourselves to the main features and the most significant differences in the optical spectra and excitonic coupling parameters obtained for the different models. The data for all excitonic couplings between the Q_x and Q_y excitations of all investigated models and the corresponding uncoupled and coupled spectra can be found in the Supporting Information.

3.3.1. Excitonic Couplings. Table 1 lists the absolute values of the Q_y coupling constants for the complete optP structures obtained with local excitations from an FDEu-pocket calculation and the all-10-Å-model. We find, in general, similar exciton coupling parameters for the two models. The largest excitonic coupling (21 meV/20 meV) is obtained for the Q_y excitations of the pigment pair BChl 371—BChl 372. Those for BChl 373—BChl 374, BChl 374—BChl 375, BChl 375—BChl 376, and BChl 374—BChl 377 are of the order of 10 meV. Interpigment couplings between Q_y and Q_x excitation can be of the same order (see Figure 3). Thus, constraining the effective exciton treatment to Q_y states only seems not to be generally justified. The relative Q_y excitonic couplings calculated here are in line with reported values obtained with the dipole−dipole approximation[12] and the TrEsp method for the 3ENI structure,[13] respectively. However, the FDEc coupling parameters tend to be larger, especially in case of strong couplings. This might be rationalized by the scaling of the oscillator strengths and excitonic couplings in the previous studies, whereas no scaling parameters were applied in this work.

An analysis of all sets of excitonic coupling parameters (see the Supporting Information) reveals that the excitonic coupling constants are rather stable upon changing the structural model or the computational details in the generation of the local transition densities. For instance, the exciton interactions for the strongest coupling, which occurs between the Q_y excitations of BChl 371 and BChl 372, lie between 19 and 22 meV in all cases. A spread of up to 4 meV is a typical value found for several couplings. However, there are also outliers. These are typically obtained with the B-D optA structures. In a few cases for optA structures, considerable excitonic couplings of Q excitations to excitations outside the Q manifold have been observed. This indicates, similar to what has been reported in

Table 1. Absolute Values of Calculated Excitonic Coupling Constants in meV in Between the Q_y Excitations for the Complete optP Structures with FDEu Pocket Local Excitations and the All-10-Å-Model and Previously Reported Data by Schmidt am Busch et al.[12] (for the pdb entry 3EOJ) and Olbrich et al.[13] (for the pdb entry 3ENI)

	371	372	373	374	375	376	377	378	ref.
371	—	21	1	1	1	3	1	4	this study; optP/FDEu pocket
	—	20	1	1	1	4	1	3	this study; all-10-Å-model
	—	12	1	1	1	2	2	5	12
	—	10	0	1	1	2	1	3	13
372		—	6	0	0	3	1	1	this study; optP/FDEu pocket
		—	6	2	0	3	1	0	this study; all-10-Å-model
		—	4	1	0	2	1	1	12
		—	3	1	0	1	1	0	13
373			—	9	0	1	4	0	this study; optP/FDEu pocket
			—	9	0	1	4	0	this study; all-10-Å-model
			—	7	0	1	0	0	12
			—	7	0	1	0	0	13
374				—	10	4	12	0	this study; optP/FDEu pocket
				—	10	4	11	0	this study; all-10-Å-model
				—	8	2	8	0	12
				—	7	2	6	0	13
375					—	15	2	1	this study; optP/FDEu pocket
					—	15	2	1	this study; all-10-Å-model
					—	11	1	1	12
					—	8	0	0	13
376						—	4	2	this study; optP/FDEu pocket
						—	4	2	this study; all-10-Å-model
						—	4	1	12
						—	4	0	13
377							—	2	this study; optP/FDEu pocket
							—	2	this study; all-10-Å-model
							—	1	12
							—	0	13

ref 67, that it might be necessary to include other excitations as well, which is easily possible in the FDE scheme. Nevertheless, in the more elaborate models, that is, those with the optP structures, no significant contribution of higher states has been observed, so that constraining to the Q states appears to be reasonable. The general stability of the excitonic coupling parameters fits to the observation that the coupling constants calculated for different structures (3EOJ and 3ENI) by other authors[12,13] are rather similar (see also Table 1). It is also in line with a previous study on LHC-II, which demonstrated that excitonic couplings are more robust with respect to variations in the methodology than site energies.[25] Nevertheless, one should keep in mind that according to ref 13, the excitonic couplings in the FMO protein can be quite sensitive to dynamical aspects, which are not considered in this study.

3.3.2. Coupled Spectra. In this section, we analyze the spectra resulting from the coupling of the local excitations discussed in Section 3.2. In particular, we will study the effect of the structural and environmental model chosen for the underlying local excitations on the coupled spectra. We will again restrict ourselves to a discussion of the main features and the differences obtained for different models. The complete set of data and spectra can be found in the Supporting Information.

As already discussed in the earlier sections, the coupling constants are quite stable with respect to changes in the structural model and to the treatment of the environment in the calculation of the local excitations. The site energies are more sensitive to these variations. Thus, the differences in the coupled spectra can be related to changes in site energies to a large extent and already small changes in the site energies can lead to significant differences in the electronic structure of the coupled system. First, we will discuss the influence of the structural model and subsequently that of the treatment of the environment in the calculation of the local excitation energies.

When going from the optH to optP(trunc) structures for the isolated pigments, the spectrum of the coupled Q excitations becomes narrower. This and the more pronounced mixing between the localized Q excitations can be rationalized by the smaller spread in site energies in the latter case (see Section 3.2). The more pronounced interaction also results in a broader range of oscillator strengths, that is, stronger intensity borrowing. Despite the smaller range of site energies in case of optA structures, the range of coupled excitations in the Q_y region remains similar to that of the truncated optP structures. This can be explained by the stronger interaction due to the closer energetic proximity of the local excitations. When going from the optP(trunc) structures to the complete optP structures the increased range of site energies leads also to an increased range of coupled excitations, but the distribution of oscillator strengths remains similar. Thus, only small changes in the resulting line shape are obtained for these cases.

In the results of the FDEc calculations based FDEu-network local excitations, the degree of intensity borrowing is increased compared to that based on isolated local excitations for the optH structures. In contrast to this, a decrease of the intensity borrowing is observed for the optP(trunc) structures. For the optA structures, the distribution of oscillator strengths remains similar. However, in all cases, the distribution of the local

excitations on the delocalized ones changes significantly upon going from isolated to FDEu-network local excitations. A larger change is observed when using the local excitations accounting for the environment, that is, the FDEu pocket or all-10-Å-model. In that case, the coupled excitations are more widely spread and red-shifted. This is also in line with the changes in site energies discussed in Section 3.2. Another striking difference in the FDEu pocket-based FDEc calculations to the isolated and FDEu-network calculations is that the Q_x excitation energies are shifted toward those of the Q_y excitations, so that the Q_y-Q_x gap is reduced by a factor of about two. This trend is continued when going to the larger all-10-Å-model. The Q excitations of BChl 378 couple only slightly to those of the other pigments. Thus, the spectra remain similar when adding this pigment to the network, but an additional peak arises close to the site energy of BChl 378. In the case of the coupled spectra, the localized BChl 378 Q_y transition is distributed only among excitations in close energetical proximity.

Despite the finding that the excitonic couplings are rather stable in most cases with respect to changes in the structural model and treatment of the environment in the calculation of the local excitations, the compositions of the delocalized excitations are rather sensitive against these factors. This can be mainly related to the differences in site energies discussed in Section 3.2.

4. CONCLUSIONS AND OUTLOOK

We have calculated the optical spectra of the Fenna–Matthews–Olson protein based on first-principles quantum chemistry by employing subsystem TDDFT. In particular, we have investigated the effect of the optimization strategy and the protein environment on the site energies, excitonic couplings and thus on the electronic structure within the complex. In our largest model (i.e., the all-10-Å-model), we included more than 1000 atoms of the pigment network explicitly in the FDEc calculation. Moreover, we considered a protein model comprising all residues in the radius of 10 Å from any BChl pigment. That means that more than 7000 atoms were included in the generation of the local excitations to be coupled in the FDEc calculation.

The important structural effect on the relative site energies is overestimated if the coordinates are kept constrained to the crystal structures, whereas they are underestimated for fully optimized geometries. To meet the requirement of both, a physically reasonable local structure and the constraints induced by the natural environment, we optimized all complete BChl pigments separately in their individual binding pocket comprising more than 1000 atoms in several cases. A comparison of the site energies for these structures to those from the nonoptimized and fully optimized structures suggests that the nonoptimized structures might be advantageous over the fully optimized structures. Nevertheless, one should be aware of the possibility of different effects of a geometry optimization on the site energies for different pigments. Thus, a geometry optimization with sufficient constraints, such as in a binding pocket, is still recommended, where applicable.

Our probably best data for site energies (i.e., that for the all-10-Å-model) are higher than the previously reported ones.[12,13] In view of the typical error range of excitation energies calculated with TDDFT and the fact that we, contrary to other authors,[12] did not employ scaling factors for the excitation energies, this is not unexpected. The range of site energies we calculated is of the same order of magnitude, though somewhat smaller than previously reported ones. Additional differences occur when the relative site energies are compared. In particular, the location of the exit pigment is different from that suggested in literature (see ref 4). The deviations might still be due to the truncated environment. We did not account for intact protein helices, which were argued in refs 29 and 38 to be an important factor. Results by Olbrich et al.,[13] however, suggest that also accounting for dynamical aspects might be important. Thus, the determination of site energies without system-specific parameters remains challenging.

In contrast to that, the excitonic coupling constants appear to be rather insensitive to the technical parameters analyzed here, and their relative values compare quite well to those previously reported.[12,13] We do not expect full quantitative agreement of the exciton coupling parameters to the previous studies, as the latter employ empirically scaled oscillator strengths and coupling constants. Here, we do not account explicitly for the screening of the exciton couplings by the protein. The effect of the protein is included explicitly in the local excitations from FDEu calculations; that is, we use transition densities polarized by the protein. Still, no differential polarization effects of the protein on the excitations are included. Despite the rather stable exciton coupling parameters, the electronic structure within the BChl network in the FMO protein is quite sensitive to technical parameters. In particular, the distribution of oscillator strengths and the composition of the delocalized excitations change when varying technical parameters. These differences are apparently mainly caused by changes in calculated site energies.

In view of the different sets of site energies that can be found in the literature and the impact these differences have on the electronic structure and the exciton kinetics,[68] a reliable determination of these excitation energies is one of the main challenges for understanding the initial steps in photosynthetic light harvesting from first principles. FDE is a promising approach free of system-specific parameters for the calculation of optical spectra of pigment–protein complexes. The independence of system-specific parameters is a great advantage over other approaches as it increases the predictive power of this approach. Still, the interplay of parameters affecting the electronic structure of light-harvesting complexes is quite complex. Hence, more experience is required to understand how the subtle but important choices made in the model setup affect the electronic structure. In view of the structural aspects, it could be interesting to combine FDE with molecular dynamics as similarly done for thermodynamic calculations on a ground state problem[69] and for optical spectra of similar protein–pigment complexes with other approaches.[13,68] To assess the convergence with the size of the environment, it could be instructional to systematically investigate the site energies obtained with increasing size of the environment. When going to bigger systems, the question of the protonation pattern needs to be reinvestigated, since the screening should be better in larger systems. Possible charges could also be compensated by a continuum solvation model around the explicit environment taken into account. These will be the next important steps toward a realistic and fully quantum chemical description of light-harvesting complexes.

■ ASSOCIATED CONTENT

Supporting Information

Excitation energies and oscillator strengths calculated for different models of the BChl pigments and treatment of the environment discussed in the main text; overview of the range of these parameters spanned for the different setups. Delocalized Q excitations, their composition from localized excitations, excitonic couplings, and optical spectra for each model. This information is available free of charge via the Internet at http://pubs.acs.org/.

■ AUTHOR INFORMATION

Corresponding Author

*E-mail: j.neugebauer@uni-muenster.de.

Notes

The authors declare no competing financial interest.

■ ACKNOWLEDGMENTS

We would like to thank Prof. Marcus Elstner for providing DFTB parameters for Mg. This work was supported by a VIDI grant (700.59.422) of The Netherlands Organization for Scientific Research (NWO) and a computer time grant from The Netherlands National Computing Facilities Foundation (NCF).

■ REFERENCES

(1) Fenna, R. E.; Matthews, B. W. *Nature* **1975**, *258*, 573−577.
(2) Matthews, B. W.; Fenna, R. E.; Bolognesi, M. C.; Schmid, M. F.; Olson, J. M. *J. Mol. Biol.* **1979**, *131*, 259−285.
(3) Blankenship, R. E. *Molecular Mechanisms of Photosynthesis*; Blackwell Science: Oxford, 2002.
(4) Milder, M. T. W.; Brüggemann, B.; van Grondelle, R.; Herek, J. L. *Photosynth. Res.* **2010**, *104*, 257−274.
(5) Tronrud, D. E.; Wen, J.; Gay, L.; Blankenship, R. E. *Photosynth. Res.* **2009**, *100*, 79−87.
(6) Wen, J.; Zhang, H.; Gross, M. L.; Blankenship, R. E. *Biochemistry* **2011**, *50*, 3502−3511.
(7) van Grondelle, R.; Novoderezhkin, V. I. *Phys. Chem. Chem. Phys.* **2006**, *8*, 793−807.
(8) Renger, T. *Photosynth. Res.* **2009**, *102*, 471−485.
(9) König, C.; Neugebauer, J. *ChemPhysChem* **2012**, *13*, 386−425.
(10) Ritschel, G.; Roden, J.; Strunz, W. T.; Aspuru-Guzik, A.; Eisfeld, A. *J. Phys. Chem. Lett.* **2011**, *2*, 2912−2917.
(11) Brixner, T.; Stenger, J.; Vaswani, H. M.; Cho, M.; Blankenship, R. E.; Fleming, G. R. *Nature* **2005**, *434*, 625−628.
(12) Schmidt am Busch, M.; Müh, F.; Madjet, M. E.; Renger, T. *J. Phys. Chem. Lett.* **2011**, *2*, 93−98.
(13) Olbrich, C.; Jansen, T. L. C.; Liebers, J.; Aghtar, M.; Strümpfer, J.; Schulten, K.; Knoester, J.; Kleinekathöfer, U. *J. Phys. Chem. B* **2011**, *115*, 8609−8621.
(14) Wendling, M.; Przyjalgowski, M.; Gülen, D.; Vulto, S.; Aartsma, T. J.; van Grondelle, R.; van Amerongen, H. *Photosynth. Res.* **2002**, *71*, 99−123.
(15) van Stokkum, I. H. M.; Papagiannakis, E.; Vengris, M.; Salverda, J. M.; Polívka, T.; Zigmantas, D.; Larsen, D. S.; Lampoura, S. S.; Hiller, R. G.; van Grondelle, R. *Chem. Phys.* **2009**, *357*, 70−78.
(16) Berlin, Y.; Burin, A.; Friedrich, J.; Köhler, J. *Phys. Life Rev.* **2007**, *4*, 64−89.
(17) van der Weij-de Wit, C. D.; Dekker, J. P.; van Grondelle, R.; van Stokkum, I. H. M. *J. Phys. Chem. A* **2011**, *115*, 3947−3956.
(18) Buda, F. *Photosynth. Res.* **2009**, *102*, 437−441.
(19) Pflock, T. J.; Oellerich, S.; Krapf, L.; Southall, J.; Cogdell, R. J.; Ullmann, G. M.; Köhler, J. *J. Phys. Chem. B* **2011**, *115*, 8821−8831.
(20) Wesolowski, T. A.; Warshel, A. *J. Phys. Chem.* **1993**, *97*, 8050−8053.
(21) Casida, M. E.; Wesołowski, T. A. *Int. J. Quantum Chem.* **2004**, *96*, 577−588.
(22) Neugebauer, J. *J. Chem. Phys.* **2007**, *126*, 134116.
(23) Neugebauer, J. *J. Phys. Chem. B* **2008**, *112*, 2207−2217.
(24) Neugebauer, J.; Curutchet, C.; Muños-Losa, A.; Mennucci, B. *J. Chem. Theory Comput.* **2010**, *6*, 1843−1851.
(25) König, C.; Neugebauer, J. *Phys. Chem. Chem. Phys.* **2011**, *13*, 10475−10490.
(26) Adolphs, J.; Renger, T. *Biophys. J.* **2006**, *91*, 2778−2797.
(27) Adolphs, J.; Müh, F.; Madjet, M. E.; Renger, T. *Photosyn. Res.* **2008**, *95*, 197−209.
(28) Adolphs, J.; Müh, F.; Madjet, M. E.; Schmidt am Busch, M.; Renger, T. *J. Am. Chem. Soc.* **2010**, *132*, 3331−3343.
(29) Müh, F.; Madjet, M. E.; Renger, T. *J. Phys. Chem. B* **2010**, *114*, 13517−13535.
(30) Gudowska-Nowak, E.; Newton, M. D.; Fajer, J. *J. Phys. Chem.* **1990**, *94*, 5795−5801.
(31) Linnato, J.; Korppi-Tommola, J. *J. Phys. Chem. A* **2004**, *108*, 5872−5882.
(32) Linnato, J.; Korppi-Tommola, J. *Phys. Chem. Chem. Phys.* **2006**, *8*, 663−687.
(33) Zucchelli, G.; Brogioli, D.; Casazza, A. P.; Garlaschi, F. M.; Jennings, R. C. *Biophys. J.* **2007**, *93*, 2240−2254.
(34) Zucchelli, G.; Santabarbara, S.; Jennings, R. C. *Biochemistry* **2012**, *51*, 2717−2736.
(35) Dreuw, A.; Harbach, P. H. P.; Mewes, J. M.; Wormit, M. *Theor. Chem. Acc.* **2010**, *125*, 419−426.
(36) Warshel, A.; Sharma, P. K.; Kato, M.; Parson, W. W. *Biochim. Biophys. Acta* **2006**, *1764*, 1647−1676.
(37) Alden, R. G.; Parson, W. W.; Chu, Z. T.; Warshel, A. *J. Am. Chem. Soc.* **1995**, *117*, 12284−12298.
(38) Müh, F.; Madjet, M. E.; Adolphs, J.; Abdurahman, A.; Rabenstein, B.; Ishikita, H.; Knapp, E.-W.; Renger, T. *Proc. Natl. Acad. Sci. U.S.A.* **2007**, *104*, 16862−16567.
(39) Åqvist, J.; Luecke, H.; Quiocho, F. A.; Warshel, A. *Proc. Natl. Acad. Sci. U.S.A.* **1991**, *88*, 2026−2030.
(40) Luzhkov, V.; Warshel, A. *J. Am. Chem. Soc.* **1991**, *113*, 4491−4499.
(41) Warshel, A.; Chu, Z. T. *J. Phys. Chem. B* **2001**, *105*, 9857−9871.
(42) Förster, T. *Ann. Phys.* **1948**, *437*, 55−75.
(43) Andrews, D. L.; Curutchet, C.; Scholes, G. D. *Laser Photonics Rev.* **2011**, *5*, 114−123.
(44) Madjet, M. E.; Abdurahman, A.; Renger, T. *J. Phys. Chem. B* **2006**, *110*, 17268−17281.
(45) Ahlrichs, R.; Bär, M.; Häser, M.; Horn, H.; Kölmel, C. *Chem. Phys. Lett.* **1989**, *162*, 165−169.
(46) Becke, A. D. *Phys. Rev. A* **1988**, *38*, 3098−3100.
(47) Perdew, J. P. *Phys. Rev. B* **1986**, *33*, 8822−8824.
(48) Harris, J. *Phys. Rev. B* **1985**, *31*, 1770−1779.
(49) Foulkes, W. M. C.; Haydock, R. *Phys. Rev. B* **1989**, *39*, 12520−12536.
(50) Cai, Z.-L.; Lopez, P.; Reimers, J. R.; Cui, Q.; Elstner, M. *J. Phys. Chem. A* **2007**, *111*, 5743−5750.
(51) Swart, M.; Bickelhaupt, F. M. *J. Comput. Chem.* **2008**, *29*, 724−734.
(52) Te Velde, G.; Bickelhaupt, F. M.; Baerends, E. J.; Fonseca Guerra, C.; van Gisbergen, S. J. A.; Snijders, J. G.; Ziegler, T. *J. Comput. Chem.* **2001**, *22*, 931−967.
(53) Schipper, P. R. T.; Gritsenko, O. V.; van Gisbergen, S. J. A.; Baerends, E. J. *J. Chem. Phys.* **2000**, *112*, 1344−1352.
(54) Gritsenko, O. V.; Schipper, P. R. T.; Baerends, E. J. *Chem. Phys. Lett.* **1999**, *302*, 199−207.
(55) Gritsenko, O. V.; Schipper, P. R. T.; Baerends, E. J. *Int. J. Quantum Chem.* **2000**, *76*, 407−419.
(56) Wesolowski, T. A. *J. Chem. Phys.* **1997**, *106*, 8516−8526.
(57) Neugebauer, J.; Jacob, C. R.; Wesolowski, T. A.; Baerends, E. J. *J. Phys. Chem. A* **2005**, *109*, 7805−7814.
(58) Jacob, C. R.; Neugebauer, J.; Visscher, L. *J. Comput. Chem.* **2008**, *29*, 1011−1018.

(59) Wesolowski, T. A.; Weber, J. *Chem. Phys. Lett.* **1996**, *248*, 71−76.
(60) Sundholm, D. *Chem. Phys. Lett.* **2000**, *317*, 545−552.
(61) Linnato, J.; Korppi-Tommola, J. *Phys. Chem. Chem. Phys.* **2000**, *2*, 4962−4970.
(62) Linnato, J.; Korppi-Tommola, J. *J. Comput. Chem.* **2004**, *25*, 123−137.
(63) Louwe, R. J. W.; Vrieze, J.; Hoff, A. J.; Aartsma, T. J. *J. Phys. Chem. B* **1997**, *101*, 11280−11287.
(64) Larson, C. R.; Seng, C. O.; Lauman, L.; Matthies, H. J.; Wen, J.; Blankenship, R. E.; Allen, J. P. *Photosynth. Res.* **2011**, *107*, 139−150.
(65) Jacquemin, D.; Wathelet, V.; Perpète, E. A.; Adamo, C. *J. Chem. Theory Comput.* **2009**, *5*, 2420−2435.
(66) Renaud, N.; Ratner, M. A.; Mujica, V. *J. Chem. Phys.* **2011**, *135*, 075102.
(67) Shibata, Y.; Tateishi, S.; Nakabayashi, S.; Itoh, S.; Tamiaki, H. *Biochemistry* **2010**, *49*, 7504−7515.
(68) Shim, S.; Rebentrost, P.; Valleau, S.; Aspuru-Guzik, A. *Biophys. J.* **2012**, *102*, 649−660.
(69) Olsson, M. H. M.; Hong, G.; Warshel, A. *J. Am. Chem. Soc.* **2003**, *125*, 5025−5039.
(70) Humphrey, W.; Dalke, A.; Schulten, K. *J. Mol. Graphics* **1996**, *14*, 33−38.